Article

Understanding the Nature of Amino Acids Interactions with Pd (111) or Pd-Au Bimetallic Catalysts in the Aqueous Phase

Madhulika Gupta, Tuhin Suvra Khan, Manish Agarwal, and M. Ali Haider

Langmuir, **Just Accepted Manuscript** • DOI: 10.1021/acs.langmuir.7b03271 • Publication Date (Web): 27 Dec 2017

Understanding the Nature of Amino Acids Interactions with Pd (111) or Pd-Au Bimetallic Catalysts in the Aqueous Phase

Madhulika Gupta,[‡, †] Tuhin S. Khan,[‡] Manish Agarwal,[¶,*] and M. Ali Haider[‡,*]

‡Renewable Energy and Chemicals Lab, *Department of Chemical Engineering, Indian Institute of Technology Delhi, Hauz Khas, Delhi-110016, India*

†*Department of Chemistry, Indian Institute of Technology Delhi, Hauz Khas Delhi-110016, India*

¶*Computer Services Centre, Indian Institute of Technology Delhi, Hauz Khas, Delhi-110016, India*

**Corresponding authors*

E-mail: haider@iitd.ac.in, zmanish@cc.iitd.ac.in

Abstract

Interaction of Methionine (Met) with different bimetallic-segregated surfaces comprising of uniform distribution, strips and islands of Au on Pd (111) surface were examined using molecular dynamics (MD) simulations. Out of all the segregated and uniformly doped surfaces studied, the design of Pd-Au islands showed some reduction in the interaction energy (E_{int}= -43.7 kJ/mol) as compared to the pure Pd (111) surface (E_{int}= -50 kJ/mol) for a single Met molecule. However, at a higher coverage of 9 Met molecules/simulation cell, none of the Pd-Au alloy surfaces showed any improvement as compared to the Pd (111) surface. In order to develop a comprehensive understanding on the nature of non-bonded interaction of aqueous biogenic impurities with the Pd catalyst surface, the MD study was extended to include a variety of aliphatic, S-containing, aromatic and polar amino acids. The potential of mean force (PMF) profiles were observed to be distinct for each class of amino acids with substantial differences among amino acids with acidic and basic side chains. The side chains of all the polar and aromatic amino acids showed direct contact with the surface while aliphatic amino acids had their hydrophobic side chain aligned away from the surface. Interestingly, Lysine (Lys) and Tyrosine (Tyr) were the only two amino acids, which interacted preferentially via the distant backbone nitrogen and backbone oxygen, respectively, despite their side-chain being in direct contact with the metal surface. The strength of interaction was correlated with the size of the

amino acid; the interaction energies were observed to be the maximum for large molecules like Arginine (Arg, E_{int} =-87.7 kJ/mol) and Tryptophan (Trp, E_{int} = -73.4 kJ/mol), while it was minimum for aliphatic amino acids like Alanine (Ala, E_{int}=-10.9 kJ/mol). The study is focused on examining the sensitivity of the choice of the preferential interaction site, conformational preferences and interaction energies to the side chain specificity.

Key words: heterogeneous catalysis, biogenic impurities, transition metal catalysts, bimetallic catalysts, amino acids, molecular simulations

Introduction

In the development of processes for the production of biomass-derived renewable fuels and chemicals, possibilities are explored to integrate two different extremes of bio- and chemo-catalysis, wherein fermentation-derived platform molecules are converted into high value products via heterogeneously catalyzed reactions. This unique integration offers opportunities for fundamental and applied research in both areas, which has been reviewed recently by Shanks, Dumesic and co-workers [1,2]. For example, in heterogeneous catalysis, the reactions were earlier studied for vapor-phase and high temperature-pressure conditions to functionalize fossil fuel derived hydrocarbons [3–5]. In contrast, now for biorenewable chemicals, the focus is on studying reactions in aqueous phase and at mild temperature-pressure conditions, with an objective to de-functionalize biomass-derived highly oxygenated platform molecules [2,4,6]. While the option to explore novel routes for the synthesis of biorenewable chemicals and fuels is interesting and intriguing, the challenge in successful integration of the two technologies, to produce a desired product, still holds the key to commercial success. This challenge could be completely different and relatively unexplored in nature. For example, Miller and co-workers first studied the presence of small traceable amount (50 ppm) of fermentation derived biogenic impurities (amino acids for example, Met) to be detrimental for the stability of a transition metal (Ru) catalyst for hydrogenation reaction of the fermentation-derived lactic acid [7]. This was further corroborated by the experiments of Dumesic group on the hydrogenation of triacetic acid lactone (TAL), wherein a similar deactivation of the Pd catalyst was observed in presence of the biogenic (Met) impurity [2].

In order to overcome this challenge and to reduce the effect of biogenic impurity in catalyst deactivation, the obvious alloying strategy of preparing a bimetallic Pd-Au alloy catalyst was explored, which was expected to improve catalyst stability, by destabilizing the interaction of the impurity with the metal surface [8]. Surprisingly, compared to the monometallic catalyst, this alloy did not show any improvement in catalyst deactivation in presence of the amino acid (Met) impurity. In our recently published theoretical work on the interaction of biogenic impurities with the Ni catalyst surface, we have attempted to elucidate the nature of both bonding and non-bonding interactions of a variety of amino acids with the Ni catalyst surface [9]. In this, a possible reason for the deactivation of the Pd-Au bimetallic was cursorily explored using DFT calculations of Met binding on Pd and 1:1 homogeneous Pd-Au surface in the vapor phase.

However, our explanation remained inconclusive, since the interaction did not include the role of aqueous phase and consequent dispersive interactions of the biogenic impurities with the Pd and/or Pd-Au catalyst surface. Moreover, in a functioning bimetallic catalyst, the idea of a homogeneous alloy surface may not be real and applicable. Vlachos and co-workers have elucidated this fact in the improved reactivity of segregated defect surfaces of bimetallic alloys for ammonia decomposition [10].

The MD study presented here is directed towards developing a comprehensive understanding on non-bonded interactions of amino acids with the Pd surface. In addition, while studying the non-bonding interactions of Met with the monometallic Pd and bimetallic Pd-Au alloy surfaces, an attempt is made to understand the nature of catalyst deactivation in the aqueous phase. To mimic a real bimetallic surface, models for segregated surfaces of Pd-Au alloy were included. Similar to the bonded electronic interactions of molecules on the catalyst surface wherein adsorption energy is well-known to decrease with increasing adsorbate coverage [3], it is expected that non-bonded dispersive interactions may also show dependence on coverage. This phenomenon is relatively less studied for applications in catalysis, which indeed is important and pertinent to explore for biogenic impurities with increased lateral interactions in aqueous phase.

In order to study these non-bonded interactions with the aforementioned objectives, sets of representative amino acids of different categories were chosen. The selection varied from 1) sulphur containing amino acids: Met and Cysteine (Cys); 2) aliphatic amino acids: Glycine (Gly), Alanine (Ala), Leucine (Leu) and Proline (Pro); 3) aromatic amino acids: Tryptophan (Trp), Histidine (His), Phenylalanine (Phe) and Tyrosine (Tyr); 4) amino acids with hydroxyl group in side chain: Threonine (Thr); 5) amino acids containing a basic side chain: Lysine (Lys) and Arginine (Arg); 6) amino acids with an acidic side chain: Glutamic acid (Glu); and 7) its amine derivative: Glutamine (Gln). The preferential interaction site of amino acid with the metal catalyst surface, thus obtained in water with MD simulations is expected to provide a fundamental basis for studying the nature of dispersive interactions of biogenic impurities with the metal catalyst surface. To the best of our knowledge, only one study conducted by us had studied this type of interactions with the transition metal catalyst surface [9]. As an extension of our previous study, we consider the development of this understanding an essential component in the design of effective catalysts for integrated fermentation and catalysis.

Simulation Details

All atom molecular dynamics (MD) simulations of different amino acids on the most stable (111) surface of Pd surface were performed using GPU-accelerated NAMD 2.10 package [11]. The metal-water interface is most relevant in such studies and hence an appropriate force field to model this interface is crucial to obtain accurate results [12,13]. In our study, CHARMM-METAL force field [14] has been used which simulated a wide range of fcc metals and their interfaces by Lennard-Jones parameters and is shown to accurately reproduce surface tension, density and interfacial tension properties with water. The initial coordinates of all the amino acids studied were generated through *Molefracture* plugin in VMD [15]. Amino acids were solvated with mTIP3P waters [16] using *solvate* plugin in VMD. All the simulations were performed with zwitter ionic form of amino acids. The side chains of Lys, Arg and Glu were modeled as per their state (neutral) in water at physiological pH [17]. A slab consisting of three atom layers was used to model Pd (111) surface which is placed at the bottom of the box and the top layer of the metal surface was denoted by z = 0. A non-orthogonal box of 33 Å × 33 Å × 33 Å was used to model Pd (111) surface. In the z direction, a space extending up to 100 Å was used in simulations so as to avoid interaction of amino acids with the periodic images of the surface in the z direction.

The solvated system was inserted onto the metal surface and the system was energy minimized for 0.5 ns using conjugate gradient method to avoid any steric strain. All the simulations were performed under NVT conditions with a time step of 1 fs. Langevin thermostat [18] with a damping coefficient of 1 ps^{-1} was used to maintain a constant temperature of 300 K. A cut-off distance of 10 Å was used for van der Waals interactions with a switch distance of 12 Å. Particle Mesh Ewald [19] was used to compute long range Coulombic interactions with a grid spacing of 1 Å. SHAKE algorithm was used to maintain all bond lengths involving hydrogen atoms [20]. In all the simulations, the metal atoms were held fixed in their lattice positions and intra-metal interactions were not taken into account. Interactions of Met on Pd-Au overlayer and different segregated surfaces were examined. The surface for Pd-Au overlayer was modeled using a monolayer of Au over three layers of Pd (111) (Figure 4(b)). The segregated surfaces (Figure 4(c)-(f)) included a uniform distribution of Pd and Au (1:1) atoms on the surface (Pd-Au uniform), single island of Au atoms on Pd surface (Pd-Au single island), multiple islands of Au on Pd surface (Pd-Au islands) and strips of Au distributed on Pd surface (Pd-Au strips). On replacing the Pd atoms

with the Au atoms, the slab surface was geometrically optimized to obtain the above mentioned 50% Pd-Au surface alloy. Simulations of Met were then performed on these surfaces.

The role of water is crucial in altering the orientation of the biogenic impurity with the metal surface. Water molecules are known to stack up over the hydrophilic metal surfaces [21–29]. In order for the amino acid to adsorb on the metal surface, it has to penetrate the water layers with simultaneous breaking of H-bonds, which is a thermodynamically nonspontaneous process. This can be captured by using non-equilibrium Steered Molecular Dynamics (SMD) simulations as shown previously by us [9] and others [30–32]. SMD approach was used to calculate interaction energies of amino acids on the different metal surfaces. In each SMD simulation, the center of mass of one or more atoms (SMD atoms) was constrained by a harmonic spring of force constant, 5000 kJ/mol/nm^2 in the z direction with a pulling velocity of 0.5 Å/ns [9]. The translational as well as rotational motions in x and y directions were not restrained. In order to explore the conformational phase space exhaustively with optimum computational efficiency, a set of ten different orientations of the amino acids was chosen, thereby acting as representatives of rotational sampling. The tagged sites were located more than 17-20 Å away from the metal surface in the initial configurations. The potential of mean force (PMF) can be calculated by a quasi-static approach which involves a mathematical integration of the forces along a constrained direction (z) [33]. The PMF was calculated by mathematically integrating the constrained forces along the z direction. The minima in the PMF corresponded to the interaction energy of amino acid and its location defines the vertical distance between the interacting site (center of mass of one or more SMD atoms) of the amino acid and the metal surface. Since configurations likely to interact strongly with the catalyst surface were of interest, the reported interaction energies were calculated by taking an average over best five energies (most negative) from the PMF profiles. A detailed description of using this bias of best five interaction energies to represent those trajectories, which interacted strongly with the catalyst surface, is available in the report by Madhulika et al. [9]

Interaction of amino acids through all the potential interaction sites (non-hydrogen and non-carbon) were examined by tagging each site individually in SMD simulations. Figure 1 shows all the tagged sites highlighted in blue color for the respective amino acid. Interactions through backbone atoms; nitrogen (N_{bb}) and two carboxyl oxygens ($O1_{bb}$, $O2_{bb}$) were examined in all the

cases. For aromatic amino acids, in addition to backbone atoms, the ring itself (Ring), nitrogen(s) present in the ring (RingN) or oxygen(s) present in the ring (RingO) can act as potential interaction sites. In addition, interactions by tagging sulfur (S), nitrogen (N_S, N_{S1}, N_{S2}) or oxygen (O_S, O_{S1}, O_{S2}) present in the side chains of amino acids were included. The site of the amino acid, which interacted with the highest interaction energy (most negative), was considered to be the preferential interaction site with the metal surface. The interactions through the preferential interaction site are discussed in the results section. The interactions via other sites were relatively weak and all the interaction energies for all the sites are reported in Tables S1 and S2 of supplementary information. In order to ensure the stability of the conformation, which interacted with the metal surface through different potential interaction sites, extended runs of 10 ns were performed, by choosing that specific configuration.

Results and Discussion

Solvent density profile

The water density profile above Pd (111) surface as shown in Figure S1 depicts the stacking of water molecules in two distinct layers at 3 and 6 Å and a weakly ordered third layer at 9 Å above the metal surface. The arrangement of water molecules in ordered layers above Pd surface is similar to that observed for the Ni and other hydrophilic surfaces [9,21–23,25–29,34], confirming to the hydrophilicity of the Pd surface. In order for the amino acids to interact with the Pd (111) surface, the penetration of these water layers is essential.

Interaction of Met on Pd (111) surface and Pd-Au overlayer

On applying the same method, MD simulations elucidated the non-bonded interaction of Met with the Pd surface. Met is known to irreversibly poison Ni, Pd and Pt surfaces due to presence of S in the side chain [3]. The study on Ni (111) surface also corroborated to the strong interaction of Met with the metal surface via the S atom present in the side chain [9]. The interaction energy of backbone atoms, N_{bb}, $O1_{bb}$ and $O2_{bb}$ of Met with the Pd (111) surface varied between -24 to -32 kJ/mol as shown in Table S1. On comparing the interaction energies of various polar sites of Met, it was observed that Met showed maximum interaction on Pd surface via S present in the side chain with E_{int} = -50 kJ/mol as shown in Table 1. Thus, S was the preferred interaction site for Met on the Pd surface. On visual inspection, it was revealed that Met oriented parallel to the

metal surface with S at a distance of ~3.0 Å from the surface. A representative snapshot is shown in Figure 2(a). The corresponding PMF profile averaged over top 5 runs is shown in Figure 3(a). The locations for undulations observed in the PMF profile correspond to the crossing of the two ordered layers and the weakly ordered third water layer above the metal surface. It was evident from Table 1 that the non-bonded interaction energy of Met via S atom on the Pd surface was relatively strong. Combined with our previously reported DFT calculated value (E_{ads} = -100 kJ/mol) of Met adsorption on Pd (111), it is substantiated that such strong interactions of a biogenic impurity may result into the irreversible poisoning of the catalyst surface, as observed in the experiments [3]. Not only Pd, Dumesic and co-workers had reported that all the three prominent transition metal catalysts (Ni, Pd and Pt), used for hydrogenation and hydrodeoxygenation reactions, are likely to deactivate irreversibly in presence of Met [3].

For the Ni, Pd or other such transition metal catalyst, alloying with Au is a known option in heterogeneous catalysis to destabilize the formation of carbon, and thus coke formation, on the catalyst surface [35]. Au, as the noble element is expected to alter the electronic environment around Pd or Ni catalyst in a favorable way to provide lesser binding of carbon or other such adsorbed species. This prompted experiments to synthesize Pd-Au bimetallic catalyst for TAL hydrogenation in presence of Met. Unfortunately, no appreciable improvement in catalyst stability during the time on stream was observed [36]. DFT calculations elucidated the reason for the same wherein binding energy of Met and S on 1:1 Pd-Au surface alloy catalyst (E_{bind} = -103 kJ/mol and -546 kJ/mol, respectively) were observed to be similar to the Pd surface (E_{bind} = -100 kJ/mol and -541 kJ/mol, respectively) [9]. Since Au is inert and is not suitable to be used in hydrogenation and other reactions, calculations on pure Au (111) surface were not performed [37,38]. Instead, calculations for Pd-Au overlayer showed that Met interacted with the metal surface through the S atom present in side chain with E_{int} = -42.9 kJ/mol at a distance of 3.0 Å from the surface as shown in Table 2. The orientation of the S atom of Met on Pd-Au overlayer in best five runs is shown in Figure 4(b) where the S atom oriented at the hollow site formed by three Pd neighbors. The non-bonded interactions of Met with the Pd-Au bimetallic alloys further reveals the nature of dispersive interaction in aqueous phase. Met interacted with the uniform Pd-Au alloy surface, as shown in Figure 4(c), through the S atom with E_{int} = -50.3 kJ/mol at a distance of 3.1 Å as given in Table 2. The positioning of the interacting site, i.e., the S atom of Met in the

best five runs is shown in Figure 4(c) for the Pd-Au uniform surface. It was evident that S atom of Met interacted favorably with Pd as compared to Au atoms on the surface. The non-bonding interaction energy of Met on Pd-Au uniform surface is comparable to pure Pd surface (Table 2).

Interaction of Met on segregated Pd-Au surfaces

Pioneering work by Vlachos and co-workers has shown the effect of defect and segregated surfaces in the form of patches in bimetallic alloys, which significantly alters the activity of the catalyst surface, by exposing certain active facets more than the other [10]. One thought to engineer the bimetallic surface may employ such a design of catalyst surface, wherein segregated patches of Au in a Pd-Au alloy may destabilize interactions with a biogenic impurity. To study this, different models of segregated Pd-Au surface were employed. This may further elucidate the reason for the deactivation of a real bimetallic alloy catalyst, where ideal homogeneously uniform bimetallic surface models may not be consistent with the experimental observations. First, the interaction of Met was examined on Pd-Au strips where strips of Au were arranged on Pd surface as shown in Figure 4(d). Met interacted with Pd-Au strips with E_{int} = -48.2 kJ/mol via S atom at a distance of 3.1 Å from the surface as shown in Table 2. The S atom interacted with the Pd surface preferentially by orienting at the hollow site formed by three Pd atoms as observed in Figure 4(d). This behavior was consistent with one observed for Pd (111) surface (Figure 4(a)). It is evident that akin to Pd-Au uniform surface, Pd-Au strips also showed similar interaction energy for Met as compared to the Pd surface. In search of a better design of bimetallic surface, a variety of patches of Au on Pd surface were explored where Au arranged as a single island on Pd surface (Pd-Au single island) as well as in the form of multiple small islands (Pd-Au islands) were studied, as shown in Figures 4(e) and (f), respectively. Met interacted with Pd-Au single island with E_{int} = -50.2 kJ/mol and S at a distance of 3.1 Å from the surface as shown in Table 2. While for Pd-Au multiple islands, E_{int} was slightly reduced to -43.7 kJ/mol with S atom preferentially oriented towards the surface and lying at 3.1 Å above the surface. This value is comparable to the interaction energy values for Met on Pd-Au overlayer with S as the preferential interaction site. In general, it was observed that all the surfaces studied showed comparable interaction energies as that for pure Pd (111) i.e., around -50 kJ/mol. The orientation of the S site of Met in the top 5 runs for Pd-Au single island showed similar placement for the S site in a 3-site triad formed by Pd atoms. Interestingly, only in one of the

simulations out of best five, similar orientation of the S site was observed with three Au atoms instead of Pd, as shown in Figure 4(e). In order to investigate this further, ten additional simulations were performed for interaction of Met on Pd-Au single island. Consistently, S was surrounded by three Pd atoms in all of the simulations. Hence, the positioning of S atom with three Au neighbors is a rare event which was captured in one of our simulations. For Pd-Au islands, S site of Met oriented near the Pd surface in all the simulations as depicted in Figure 4(f). Since the S site of Met preferentially interacted with the Pd, alloying in any form of the Pd surface with Au was calculated to show similar interaction energy.

Interaction energies as a function of coverage on different surfaces

Bonded interactions of surface adsorbates on a metal catalyst surface show a significant reduction in binding energies with increased lateral interaction [9,39–42]. A specific design of bimetallic surface at low coverage, to destabilize interaction with the impurity, may very-well behave differently at high coverage. It is therefore essential to examine the change in interaction energies of biogenic impurities as a function of increase in the number of such molecules on the surface. To obtain further insights, calculations for multiple Met molecules were performed for pure Pd, Pd-Au uniform, Pd-Au strips and Pd-Au islands. Figure 5 shows that the calculated interaction energies values were similar on Pd-Au uniform and Pd-Au strips for a coverage of 3 Met molecules/simulation cell, while pure Pd and Pd-Au islands showed a decrease in interaction energies. With further increase in coverage, it was observed that Pd-Au islands show a gradual decrease in E_{int} up to 7 Met molecules/ simulation cell as compared to other surfaces. For 9 Met molecules/ simulation cell on the surface, pure Pd (111) surface showed lowest E_{int} values as compared to other surfaces. It may be noted that 9 Met molecules/simulation cell was likely the limit of first monolayer dispersive interaction in the aqueous phase. It is evident from these studies that on increasing the coverage, Pd (111) will perform comparable to other surfaces, further alluding to the fact that Pd-Au alloying did not improve upon catalyst deactivation as compared to the Pd catalyst. Since these surfaces do not show any marked improvement in the interaction with the catalyst surface, the non-bonding interactions of other amino acids were examined on pure Pd (111) surface only, as discussed hereafter.

Interaction of S-containing and aliphatic amino acids with Pd (111) surface

The other S-containing amino acid, Cys, showed a similar orientation as of Met but with a lower interaction energy than Met (Met>Cys). Cys showed maximum interaction via S present in the side chain with E_{int} of -40.2 kJ/mol as shown in Table 1. Cys side chain oriented parallel to the metal surface with S at a distance of ~3.0 Å from the surface as shown in Figure 2(b). The corresponding PMF profile is shown in Figure 3(a). The interactions via backbone atoms were low and mostly comparable to Met as shown in Table S1. The next choice of amino acids was a selection of aliphatic amino acids comprising of Gly, Ala and Leu. All of them were observed to interact with the metal surface with $O2_{bb}$ as the preferred interaction site. The interaction energy values were -21.8, -15 and -16.5 kJ/mol for Gly, Ala and Leu, respectively, as shown in Table 1. Representative configurations are shown in Figures 2(c)-(e) where methyl or methylene side chain oriented away from the metal surface while the backbone atoms oriented towards the surface. A similar orientation of Ala was observed in the MD and DFT studies on the Ni, Pt and Au surfaces [9,21,43]. The PMF profiles as shown in Figure 3(b) are qualitatively similar for Gly, Ala and Leu with respect to location of the minima corresponding to the interaction energy at 2.8 Å and one at 5.5 Å depicting penetration into the depletion layer between the two ordered water layers above the metal surface. Another example of aliphatic amino acid is Pro containing a cyclic, rigid, five-membered pyrrolidine ring. Pro showed different behavior as compared to other aliphatic amino acids, as shown in Figure 3(b), likely due to its unique interaction in the depletion layer. Pro was observed to interact preferentially via the ring in tilted orientations with E_{int} = 28.4 kJ/mol at a distance of 3.6 Å from the surface as shown in Table 1 and Figure 2(f). The interaction of the metal surface with the ring was comparable to the other backbone atom, $O2_{bb}$ at a distance of 2.9 Å from the surface with E_{int} value of -27.3 kJ/mol (Table S1). Despite possessing a cyclic ring, Pro did not interact with a flat oriented ring likely due to the steric strain of adjusting the torsion angles of backbone nitrogen and oxygens along with the ring on the metal surface. The cyclic structure of Pro dictated the locking of one of the torsion angle at -65° to provide conformational rigidity [44–46]. The undulations in the PMF profile can be directly related to the water density profile above the metal surface. The locations of troughs correspond to the location of the two sharp peaks in the water density profile, as shown in Figure S1. In general, the trends for the interaction energy of aliphatic amino acids can be summarized as Pro > Gly > Leu > Ala.

Interaction of aromatic amino acids with Pd (111) surface

Aromatic amino acids with heterocyclic N i.e., Trp and His are also known to be strong inhibitors of metal surface [3]. Trp showed preferential interaction via the indole ring (Ring) with E_{int} of -73.4 kJ/mol, while His preferentially interacted through the imidazole ring (Ring) with E_{int} of -48.3 kJ/mol as given in Table 1. The corresponding PMF profiles are shown in Figure 3(c). For both Trp and His, the ring was oriented parallel to the metal surface and the center of mass of the ring was located at a distance of 2.8 Å from the metal surface as shown in Figures 6(a) and (b). These results are in contrast to the observations made on Ni (111) surface wherein the heterocyclic ring nitrogen (RingN) was consistently observed to be the preferential interaction site for Trp and His rather than the heterocyclic ring (Ring) itself as observed in case of Pd (111) surface [9]. Nevertheless, these observations revealed that surface chemistry and energetics can significantly alter the preferred interaction site of an amino acid and their orientation. In few configurations, the indole ring of Trp interacted with the metal surface in tilted orientations at a distance of ~5 Å from the surface. However, the interactions were weaker in such cases due to the presence of an underlying water layer between the protein-metal interface and the ring. In contrast, His was invariably observed to interact with the surface in the flat orientation of the ring. His, despite having a bulky side chain has low steric hindrance due to nitrogens being constrained in the five-membered cyclic ring resulting in flat orientation of the ring above the metal surface [17]. Thus, conformational strain and the fit on the metal surface governs the orientation of the aromatic ring on the surface [9,17].

It is further interesting to examine amino acids which are aromatic in nature and have different functional groups substituted on the aromatic ring [47]. The aromatic ring present in Phe is hydrophobic and non-polar. Phe interacted with the Pd surface through the flat orientations of the ring (Ring) as shown in Figure 6(c) with E_{int} = -38.5 kJ/mol, oriented at a distance of 3.0 Å (Table 1) from the surface. The corresponding PMF profile is shown in Figure 3(c). Interestingly, the backbone atoms of Phe were observed to show comparable interaction energies as that of aliphatic amino acids (Table S1). DFT studies also showed that benzene ring of Phe adsorbed strongly on Group 10 metals and the ring aligned parallel to the surface [34]. Studies by Ghiringhelli and coworkers revealed that on Pt (111) surface, Phe was not able to overcome the

metal-water interactions and hence was not able to adsorb on the surface [43]. Thus, the change in side-group functionality leads to imperative differences in the nature and strength of interactions. Next, Tyr with phenolic ring as side chain was examined. Surprisingly, Tyr showed incongruous behavior as compared to other aromatic amino acids. Tyr interacted preferentially with $O1_{bb}$ followed by N_{bb} with E_{int} of -66.5 and -64.1 kJ/mol oriented at distances of 5.0 and 5.2 Å, respectively, as indicated in Tables 1 and S1. The side chain of Tyr aligned parallel to the metal surface while the preferred interaction site was observed to be $O1_{bb}$ located distant from the surface as shown in Figure 6(d). The phenolic ring interacted with Pd surface with a relatively lower E_{int} = -58.6 kJ/mol oriented at a distance of 3.0 Å followed by the oxygen present in the ring (RingO) with E_{int} = -52.1 kJ/mol oriented at a distance of 2.8 Å (Table S2). The PMF profile for Tyr is shown in Figure 3(c) for ring as tagged site so as to compare the qualitative behavior with other aromatic amino acids. The PMF profiles for Phe and Tyr are qualitatively similar while the locations of troughs vary amongst the two amino acids. Thus, E_{int} for aromatic amino acids follows the order: Trp > Tyr > His > Phe. This further illustrated that the substituents on the aromatic ring modify the choice of preferred interaction site as well as the nature of interaction.

Interaction of polar amino acids with Pd (111) surface

Polar amino acids such as Thr with a short alcohol containing side chain was studied which is known to inhibit the metal surface moderately [3]. The preferred interaction site of Thr was the side chain oxygen (O_S, Figure 1) with E_{int} value of -21.0 kJ/mol (Table 1), oriented at a distance of 2.8 Å as shown in Figure 6(e). The PMF profile is shown in Figure 3(d). Despite having a hydroxyl side chain, the interaction energy for Thr was comparable to aliphatic amino acids, possibly due to presence of methyl group in the side chain. In order to obtain a detailed understanding of the side chain specificity, the two amino acids with basic side chain, Lys and Arg were examined. Lys preferentially interacted with the Pd surface through N_{bb} with E_{int} of -52.5 kJ/mol as reported in Table 1. The PMF profile is shown in Figure 3(d). N_{bb} oriented at a distance of 4.0 Å from the surface as shown in Figure 6(f). The other basic amino acid, Arg consists of a planar δ-guanido group and interacted preferentially with side chain nitrogen (N_{S2}, Figure 1) with the E_{int} value of -87.7 kJ/mol oriented at a distance of 2.9 Å as shown in Figure 6(g) and reported in Table 1. The side chain of Arg aligned parallel to the metal surface

penetrating the penultimate water layer while N_{bb} was located in the depletion layer. The PMF profiles were observed to be very similar for Arg and Lys as shown in Figure 3(d), with a single, smooth minima corresponding to the interaction energy, unlike other amino acids. The trends for E_{int} can be stated as Arg > Lys > Thr. Glu and its amine derivative, Gln were considered next. The preferred interaction of Glu was via the side chain oxygens, O_{S1} and O_{S2} (Figure 1) with an average E_{int} of -39.8 kJ/mol at a distance of 2.8 Å (Table 1) in a flat orientation as depicted in Figure 6(h). In contrast, Gln with -$CONH_2$ in the side chain showed stronger interactions via the side chain, N_S, and backbone, N_{bb}, with a similar E_{int} value of -46 kJ/mol (Tables 1 and S1) lying at distances of 2.9 and 4.0 Å, respectively, from the surface. In such a case, the direct interaction site, N_S can be regarded as the preferred interaction site as shown in Figure 6(i). The side chain O (O_S) also interacted favorably with the metal surface (similar to N_{bb} and N_S) with E_{int} = -44.4 kJ/mol and oriented at a distance of 2.8 Å. The PMF profiles as shown in Figure 3(d) were qualitatively similar for Thr, Glu and Gln having oxygen(s) in the side-chain but quantitatively the trend in E_{int} follows the order Gln > Glu > Thr. These amino acids were stabilized by peptide-water H-bonds to a much greater extent than other amino acids and hence, more number of troughs were observed in their PMF profiles.

Summary

The interaction energies of all the amino acids through all the potential interaction sites are shown in Figure S1, confirming that all the amino acids were able to penetrate the water layer next to the surface, also termed as direct site interaction. The next possible mode of interaction of amino acids with the metal surface was through the depletion layer i.e. the amino acids interacted with the surface by orienting along the gap present between the two water layers. In such a case, the interacting site was located within a distance of 4-6 Å from the surface. Although rare (~10 of 500 simulations), some amino acids interacted with the metal surface even beyond the second water layer resulting in much weaker interactions. Interestingly, it was revealed that Arg had strongest interactions with the Pd surface followed by Trp, while Ala was least attracted to the surface. In general, the interaction energies, E_{int} of all the amino acids through their respective preferable interaction sites can be arranged as follows: Arg (N_{S2}) > Trp (Ring) > Tyr ($O1_{bb}$) > Lys (N_{bb}) > Met (S) > His (Ring) > Gln (N_S) > Cys (S) > Glu (O_{S1}, O_{S2}), Phe (Ring) > Pro (Ring) > Gly ($O2_{bb}$) > Thr (O_S) > Leu ($O2_{bb}$) > Ala ($O2_{bb}$). The amino acids with heterocyclic ring

aligned flat to the metal surface, which maximizes the dispersion effects with the planar metal surface. Most of the amino acids were observed to interact via the side chain atoms i.e., S, N, O or heterocyclic ring present in the side chain, except that of the aliphatic amino acids, Tyr and Lys. It may be noted that the preferential interaction site may not always lie in direct contact with the surface as observed for Pro, Tyr and Lys, which can be attributed to the conformational strain effects. The direct contact of any polar atom of the amino acid with the metal surface does not determine strong adsorption as was also observed by Heinz et al.[48] for the adsorption of Flg-Na_3 peptide on Au (100) and Pd (100) surfaces. On comparing the interaction energies on Pd (111) surface with the study on the Ni (111) surface [9], it was concluded that the choice of preferred site, the intrinsic conformational preferences as well as the extent of interactions of an amino acid are altered depending on the catalyst surface. The interaction energies of the same amino acids with Ni (111) surface were observed to be higher as compared to the Pd (111) surface and thus, Ni (111) is suggestively more prone to deactivation by biogenic impurities, as compared to the Pd surface [3]. This is consistent with the experimental results of Dumesic group [3].The differences in the choice of preferred site and the strength of interaction may be attributed to the surface energetics, lattice spacing, and wettability of the interacting surface.

The conformational state of the bound amino acid acquired an optimum geometry by forming hydrogen bonds with the nearby waters in order to have minimum steric strain. In general, it was observed that the side chain atoms along with $O2_{bb}$ have a tendency to lie flat on the surface while the other two backbone atoms, $O1_{bb}$ and N_{bb} lay within the depletion layer. The amino acids have inter-planar hydrogen bonding which drives the placement of these backbone atoms in different regions above the metal surface. On the other hand, aliphatic amino acids, having a hydrophobic side chain will essentially orient away from the hydrophilic metal surface [49]. This further enforces the placement of the three backbone atoms in a flat conformation above the metal surface for all the non-cyclic, aliphatic amino acids. Beyond the first two layers, the water showed homogeneous bulk-like behavior. It may further be noted that for each amino acid, the interaction energies vary corresponding to a particular tagged site but the distance between the center of mass of the site from the metal surface did not change significantly. This implies that the conformational choices were not altered for a particular amino acid, rather the interaction energies were altered depending on favorable interactions between each tagged site and the metal

surface. In order to ensure that these intrinsic conformational preferences are unique, distances of all potential adsorbing sites from the metal surface were calculated from equilibrium runs of the adsorbed configuration. In general, it was observed that none of the amino acids desorb from the surface, thus emphasizing that the geometry of the amino acid was optimum to interact with the metal surface. Interestingly, none of the simulations showed a shift in any of the relative distances of the potential interacting sites from the metal surface. This conforms to the favorable choice of the conformational state that is adopted by each amino acid to interact with the metal surface. Moreover, the interaction energy of each amino acid with the Pd surface can be correlated to the dispersion effects which in turn depends on the surface area available. Figure 7 shows the plot for solvent accessible surface area of all the amino acids as a function of their interaction energies through the preferred interaction site. It was evident that the interaction energies scale almost linearly with the available area. The observed significant deviations of Gly, Cys, Leu and Phe from the expected behavior can be attributed to the incorporated conformational flexibility of these amino acids relative to others, which might have dominated over the size effects as they approached and interacted with the catalyst surface.

Conclusions

Non-bonded dispersive interactions of biogenic impurities with the metal surface in water were studied to develop an insight on catalyst deactivation observed during catalytic transformation of fermentation-derived reactants. Heterogeneous catalyst deactivation due to carbon deposition is known to be reduced by alloying Au with the Pd catalyst. However, in case of Pd (111), both segregated and homogeneous Pd-Au model surfaces showed no improvement in destabilizing the interaction of a biogenic impurity (Met) as compared to the pure Pd (111) surface, further asserting the importance of developing a comprehensive understanding on aqueous phase interactions of a set of amino acids with the metal surface. Towards this goal, as the first step, interactions of fifteen different amino acids as representatives of aliphatic, sulfur containing, aromatic, and polar amino acids were studied with the Pd (111) surface. Different amino acids exhibit varying affinity for the surface depending on the interplay of hydrophobic and hydrophilic interactions. Analogously, since Pd (111) surface is hydrophilic, amino acids with polar side chains were exposed to the surface while aliphatic amino acids with hydrophobic side chain directed away from the surface. The amino acids interacted with the metal surface via

epitaxial site, which fitted well onto the metal surface. However, direct interaction of sub molecular fragments may not necessarily lead to preferential interactions due to resultant internal strain in the molecule. In particular, the amino acids having heterocyclic ring-N or multiple nitrogen atoms, or sulfur in the side chain showed higher interactions with the metal surface. By examining each functional group moiety, this study emphasizes upon the importance of understanding such interactions with respect to a specific chemical structure on the metal surface. The degree of interactions of different amino acids with the Pd surface cannot be generalized by classifying the categories of amino acids as aliphatic, S-containing, with aromatic, acidic or basic character. For example, the changes in the chemical structure such as Cys (thiol group) to Met (methyl-thiol group) significantly altered the interaction energy via S atom with the metal surface. Furthermore, Arg interacted most favorably with the Pd surface, closely followed by Trp while Ala was least attracted to the Pd surface.

The favored orientations of a particular amino acid near the surface is dependent on several factors including H-bonds, electrostatic and dispersion energies in conjunction with entropy gain of local waters surrounding the amino acid. The penetration of each water layer by the amino acid leads to structural organization with an optimum balance among amino acid-water and water-water hydrogen bonds. The interacting species tend to adopt a configuration which maximizes its surface interactions, and hence, the interaction energies can be directly correlated with the size of the interacting species. Amino acids with higher interaction energies were observed to have rigid and less diffusive conformational states as compared to amino acids with weak interactions. On comparing these results with the study of some of the amino acids on Ni (111) surface, it was concluded that the intrinsic choice of conformational preferences of amino acids on different metal surfaces are crucially dependent on the surface under examination. In particular, the topology which includes the lattice constant of the catalyst surface plays a governing role in dictating the suitable interaction site for an amino acid with its surface.

This study can act as a prototype to understand the interactions of any peptide sequence (and thus protein residues effect in catalyst deactivation) on the metal surface. The amino acids with strongest interaction energies will act as specific binding sites while the less interacting residues may stabilize the adsorbed state by cooperative effects involving hydrophobic interactions. This

will further open ideas on rational design of catalysts for integrated fermentation and catalysis, by destabilizing such interactions and thereby reducing the adverse effects of biogenic impurities. It would also be intriguing to examine such trends on different facets of a Pd nanoparticle including the minority Pd (100) and Pd (110) sites [50]. The effect of pH and temperature on interaction energies of amino acids on different metal surfaces is another interesting aspect, which may provide further insight.

Acknowledgement

Authors thank HPC facility of IIT Delhi for computational resources. Financial support from the Department of Biotechnology (BT/COE/34/SP15097/2015) to M.A.H. and M.G. is appreciated. M.A.H. would like to thank Bioenergy-Awards for Cutting Edge Research (BACER) Fellowship supported by the Department of Biotechnology, Government of India and the Indo-US Science and Technology Forum for his stay at the Catalysis Center for Energy Innovation (CCEI), University of Delaware, USA. Financial support to CCEI, an Energy Frontier Research Center by the U.S. Department of Energy, Office of Science, Office of Basic Energy Sciences under Award number DE-SC0001004 was helpful to M.A.H in the later stages of this manuscript during his sabbatical stay.

Supporting Information.

Brief descriptions in nonsentence format listing the contents of the files supplied as Supporting Information.

References

(1) Schwartz, T. J.; O'Neill, B. J.; Shanks, B. H.; Dumesic, J. A. Bridging the Chemical and Biological Catalysis Gap: Challenges and Outlooks for Producing Sustainable Chemicals. *ACS Catal.* **2014**, *4*, 2060–2069.

(2) Chia, M.; Schwartz, T. J.; Shanks, B. H.; Dumesic, J. A. Triacetic Acid Lactone as a Potential Biorenewable Platform Chemical. *Green Chem.* **2012**, *14*, 1850.

(3) Schwartz, T. J.; Brentzel, Z. J.; Dumesic, J. A. Inhibition of Metal Hydrogenation Catalysts by Biogenic Impurities. *Catal. Lett.* **2015**, *145*, 15–22.

(4) Alam, M. I.; Gupta, S.; Ahmad, E.; Haider, M. A. Integrated Bio- and Chemocatalytic Processing for Biorenewable Chemicals and Fuels. In *Sustainable Catalytic Processes*; Elsevier, 2015; pp 157–177.

(5) Comas, J.; Marino, F.; Laborde, M.; Amadeo, N. Bio-Ethanol Steam Reforming on Ni/Al2O3 Catalyst. *Chem. Eng. J.* **2004**, *98*, 61–68.

(6) Bozell, J. J.; Holladay, J. E.; Johnson, D.; White, J. F. *Top Value Added Chemicals from Biomass Volume I — Results of Screening for Potential Candidates from Sugars and Synthesis Gas Top Value Added Chemicals From Biomass Volume II: Results of Screening for Potential Candidates from Biorefinery Lignin*; Pacific Northwest National Laboratory: Richland, W.A., 2007.
(7) Zhang, Z.; Jackson, J. E.; Miller, D. J. Effect of Biogenic Fermentation Impurities on Lactic Acid Hydrogenation to Propylene Glycol. *Bioresour. Technol.* **2008**, *99*, 5873–5880.
(8) Bedford, N. M.; Showalter, A. R.; Woehl, T. J.; Hughes, Z. E.; Lee, S.; Reinhart, B.; Ertem, S. P.; Coughlin, E. B.; Ren, Y.; Walsh, T. R.; et al. Peptide-Directed PdAu Nanoscale Surface Segregation: Toward Controlled Bimetallic Architecture for Catalytic Materials. *ACS Nano* **2016**, *10*, 8645–8659.
(9) Gupta, M.; Khan, T. S.; Gupta, S.; Alam, I.; Agarwal, M.; Haider, M. A. Non-Bonding and Bonding Interactions of Biogenic Impurities with the Metal Catalyst and the Design of Bimetallic Alloys. *J. Catal.* **2017**, *352*, 542–556.
(10) Guo, W.; Vlachos, D. G. Patched Bimetallic Surfaces Are Active Catalysts for Ammonia Decomposition. *Nat. Commun.* **2015**, *6*, 1–7.
(11) Phillips, J. C.; Braun, R.; Wang, W.; Gumbart, J.; Tajkhorshid, E.; Villa, E.; Chipot, C.; Skeel, R. D.; Kale, L.; Schulten, K. Scalable Molecular Dynamics with NAMD. *J. Comput. Chem.* **2005**, *26*, 1781–1802.
(12) Schravendijk, P.; Vegt, N. Van Der; Site, L. D.; Kremer, K. Dual-Scale Modeling of Benzene Adsorption onto Ni (111) and Au (111) Surfaces in Explicit Water. *Chem. Phys. Chem.* **2005**, *6*, 1866–1871.
(13) Schnur, S.; Groβ, A. Properties of Metal-Water Interfaces Studied from First Principles. *New J. Phys.* **2009**, *11*, 125003.
(14) Heinz, H.; Vaia, R. A.; Farmer, B. L.; Naik, R. R. Accurate Simulation of Surfaces and Interfaces of Face-Centered Cubic Metals Using 12 - 6 and 9 - 6 Lennard-Jones Potentials. *J. Phys. Chem. C* **2008**, *112*, 17281–17290.
(15) Humphrey, W.; Dalke, A.; Schulten, K. VMD: Visual Molecular Dynamics. *J. Mol. Graph.* **1996**, *14*, 33–38.
(16) Neria, E.; Fischer, S.; Karplus, M. Simulation of Activation Free Energies in Molecular Systems. *J. Chem. Phys.* **1996**, *105*, 1902–1921.
(17) Creighton, T. E. *Proteins: Structure and Molecular Properties*; W. H. Freeman, 1992.
(18) Feller, S. E.; Zhang, Y.; Pastor, R. W.; Brooks, B. R. Constant Pressure Molecular Dynamics Simulation: The Langevin Piston Method. *J. Chem. Phys.* **1995**, *103*, 4613–4621.
(19) Darden, T.; York, D.; Pedersen, L. Particle Mesh Ewald: An N ·log(N) Method for Ewald Sums in Large Systems. *J. Chem. Phys.* **1993**, *98*, 10089–10092.
(20) Ryckaert, J. P.; Ciccotti, G.; Berendsen, H. J. C. Numerical Integration of the Cartesian Equations of Motion of a System with Constraints: Molecular Dynamics of N-Alkanes. *J. Comput. Phys.* **1977**, *23*, 327–341.
(21) Hoefling, M.; Iori, F.; Corni, S.; Gottschalk, K.-E. Interaction of Amino Acids with the Au(111) Surface: Adsorption Free Energies from Molecular Dynamics Simulations. *Langmuir* **2010**, *26*, 8347–8351.
(22) Verde, A. V.; Acres, J. M.; Maranas, J. K. Investigating the Specificity of Peptide Adsorption on Gold Using Molecular Dynamics Simulations. *Biomacromolecules* **2009**,

10, 2118–2128.
(23) Nawrocki, G.; Cieplak, M. Aqueous Amino Acids and Proteins Near the Surface of Gold in Hydrophilic and Hydrophobic Force Fields. *J. Phys. Chem. C* **2014**, *118*, 12929–12943.
(24) Nawrocki, G.; Cieplak, M. Interactions of Aqueous Amino Acids and Proteins with the (110) Surface of ZnS in Molecular Dynamics Simulations. *J. Chem. Phys.* **2014**, *140*, 95101.
(25) Huzayyin, A.; Chang, J. H.; Lian, K.; Dawson, F. Interaction of Water Molecule with Au(111) and Au(110) Surfaces under the Influence of an External Electric Field. *J. Phys. Chem. C* **2014**, *118*, 3459–3470.
(26) Monti, S.; Walsh, T. R. Free Energy Calculations of the Adsorption of Amino Acid Analogues at the Aqueous Titania Interface. *J. Phys. Chem. C* **2010**, *114*, 22197–22206.
(27) Cruz-Chu, E. R.; Aksimentiev, A.; Schulten, K. Water-Silica Force Field for Simulating Nanodevices. *J. Phys. Chem. B* **2006**, *110*, 21497–21508.
(28) Forte, G.; Grassi, A.; Marletta, G. Molecular Modeling of Oligopeptide Adsorption onto Functionalized Quartz Surfaces. *J. Phys. Chem. B* **2007**, *111*, 11237–11243.
(29) Gao, Y. K.; Traeger, F.; Shekhah, O.; Idriss, H.; Wöll, C. Journal of Colloid and Interface Science 0 Þ Probing the Interaction of the Amino Acid Alanine with the Surface of ZnO (1010). *J. Colloid Interface Sci.* **2009**, *338*, 16–21.
(30) Krammer, A.; Lu, H.; Isralewitz, B.; Schulten, K.; Vogel, V. Forced Unfolding of the Fibronectin Type III Module Reveals a Tensile Molecular Recognition Switch. *Proc. Natl. Acad. Sci.* **1999**, *96*, 1351–1356.
(31) Kosztin, D.; Izrailev, S.; Schulten, K. Unbinding of Retinoic Acid from Its Receptor Studied by Steered Molecular Dynamics. *Biophys. J.* **1999**, *76*, 188–197.
(32) Lu, H.; Isralewitz, B.; Vogel, V.; Schulten, K. Unfolding of Titin Immunoglobulin Domains by Steered Molecular Dynamics Simulation. *Biophys. J.* **1998**, *75*, 662–671.
(33) Hummer, G.; Szabo, A. Free Energy Reconstruction from Nonequilibrium Single-Molecule Pulling Experiments. *Proc. Natl. Acad. Sci.* **2001**, *98*, 3658–3661.
(34) Ghiringhelli, L. M.; Site, L. D. Phenylalanine near Inorganic Surfaces : Conformational Statistics vs Specific Chemistry. *J. Am. Chem. Soc.* **2008**, *130*, 2634–2638.
(35) Besenbacher, F.; Chorkendorff, I.; B. S. Clausen; Hammer, B.; Molenbroek, A.; Nørskov, J.; Stensgaard, I. Design of a Surface Alloy Catalyst for Steam Reforming. *Science* **1998**, *279*, 1913–1915.
(36) Schwartz, T. J.; Johnson, R. L.; Cardenas, J.; Okerlund, A.; Da Silva, N. A.; Schmidt-Rohr, K.; Dumesic, J. A. Engineering Catalyst Microenvironments for Metal-Catalyzed Hydrogenation of Biologically Derived Platform Chemicals. *Angew. Chem. Int. Ed.* **2014**, *53*, 12718–12722.
(37) Hammer, B.; Norskov, J. K. Why Gold Is the Noblest of All the Metals. *Nature* **1995**, *376*, 238–240.
(38) Mavrikakis, M.; Stoltze, P.; Nørskov, J. K. Making Gold Less Noble. *Catal. Lett.* **2000**, *64*, 101–106.
(39) Kitchin, J. R. Correlations in Coverage-Dependent Atomic Adsorption Energies on Pd(111). *Phys. Rev. B - Condens. Matter Mater. Phys.* **2009**, *79*, 1–6.
(40) Lausche, A. C.; Medford, A. J.; Khan, T. S.; Xu, Y.; Bligaard, T.; Abild-Pedersen, F.; Nørskov, J. K.; Studt, F. On the Effect of Coverage-Dependent Adsorbate-Adsorbate Interactions for CO Methanation on Transition Metal Surfaces. *J. Catal.* **2013**, *307*, 275–282.

(41) Grabow, L. C.; Hvolbæk, B.; Nørskov, J. K. Understanding Trends in Catalytic Activity : The Effect of Adsorbate – Adsorbate Interactions for CO Oxidation Over Transition Metals. **2010**, 298–310.
(42) Xu, Y.; Lausche, A. C.; Wang, S.; Khan, T. S.; Abild-Pedersen, F.; Studt, F.; Nørskov, J. K.; Bligaard, T. In Silico Search for Novel Methane Steam Reforming Catalysts. *New J. Phys.* **2013**, *15*.
(43) Ghiringhelli, L. M.; Hess, B.; van der Vegt, N. F. A.; Site, L. D. Competing Adsorption between Hydrated Peptides and Water onto Metal Surfaces : From Electronic to Conformational Properties. *J. Am. Chem. Soc.* **2008**, *130*, 13460–13464.
(44) Gupta, M.; Nayar, D.; Chakravarty, C.; Bandyopadhyay, S. Comparison of Hydration Behavior and Conformational Preferences of Trp-Cage Mini-Protein in Different Rigid-Body Water Models. *Phys. Chem. Chem. Phys.* **2016**, *18*, 32796–32813.
(45) Gupta, M.; Chakravarty, C.; Bandyopadhyay, S. Sensitivity of Protein Glass Transition to the Choice of Water Model. *J. Chem. Theory Comput.* **2016**, *12*, 5643–5655.
(46) Morris, A. L.; MacArthur, M. W.; Hutchinson, E. G.; Thornton, J. M. Stereochemical Quality of Protein Structure Coordinates. *Proteins* **1992**, *12*, 345–364.
(47) Gupta, M.; Khatua, P.; Chakravarty, C.; Bandyopadhyay, S. The Sensitivity of Folding Free Energy Landscapes of Trpzips to Mutations in the Hydrophobic Core. *Phys. Chem. Chem. Phys.* **2017**, *19*, 22813–22825.
(48) Heinz, H.; Farmer, B. L.; Pandey, R. B.; Slocik, J. M.; Patnaik, S. S.; Pachter, R.; Naik, R. R. Nature of Molecular Interactions of Peptides with Gold , Palladium , and Pd - Au Bimetal Surfaces in Aqueous Solution. *J. Am. Chem. Soc.* **2009**, *131*, 9704–9714.
(49) Dill, K. A. and Bromberg, S. *Molecular Driving Forces: Statistical Thermodynamics in Chemistry and Biology*; Garland Science, Taylor and Francis Group, 2003.
(50) Chiu, C. Y.; Wu, H.; Yao, Z.; Zhou, F.; Zhang, H.; Ozolins, V.; Huang, Y. Facet-Selective Adsorption on Noble Metal Crystals Guided by Electrostatic Potential Surfaces of Aromatic Molecules. *J. Am. Chem. Soc.* **2013**, *135*, 15489–15500.

Table 1: Interaction energies, E_{int}, for the preferred interaction site of the amino acids and distance between the interacting site and the top metal surface, D_{int}, for different amino acids on Pd (111) surface. The values in parenthesis denote the standard error in calculations.

Amino acid	Pref. site	E_{int} (kJ/mol)	D_{int} (Å)
Met	S	-50.0 (1.7)	3.0 (0.01)
Cys	S	-40.2 (4.1)	2.9 (0.01)
Gly	$O2_{bb}$	-21.8 (1.2)	2.9 (0.006)
Ala	$O2_{bb}$	-15.0 (1.4)	2.8 (0.008)
Leu	$O2_{bb}$	-16.5 (2.3)	2.8 (0.62)
Pro	Ring	-28.4 (0.4)	3.6 (0.05)
Trp	Ring	-73.4 (7.8)	2.9 (0.002)
His	Ring	-48.3 (1.1)	2.9 (0.02)
Phe	Ring	-38.5 (3.7)	3.0 (0.02)
Tyr	$O1_{bb}$	-66.5 (3.0)	5.0 (0.33)
Thr	O_S	-21.0 (2.2)	2.8 (0.03)
Lys	N_{bb}	-52.5 (3.0)	4.0 (0.10)
Arg	N_{S2}	-87.7 (1.2)	2.9 (0.002)
Glu	O_{S1},O_{S2}	-39.8 (3.6)	2.8 (0.01)
Gln	N_S	-45.7 (3.8)	2.9 (0.01)

Table 2: Interaction energies, E_{int}, for Met on different surfaces. The values in parenthesis denote the standard error in calculations. The distance between the S atom of Met and Pd (111) surface/ Pd-Au overlayer is 3.0 Å while for the other listed metal surfaces is 3.1 Å .

	Pd (111)	Pd-Au overlayer	Pd-Au Uniform	Pd-Au Strips	Pd-Au Single Island	Pd-Au Islands
E_{int} (kJ/mol)	-50.0 (1.7)	-42.9 (1.4)	-50.3 (1.5)	-48.2 (3.2)	-50.2 (2.0)	-43.7 (1.8)

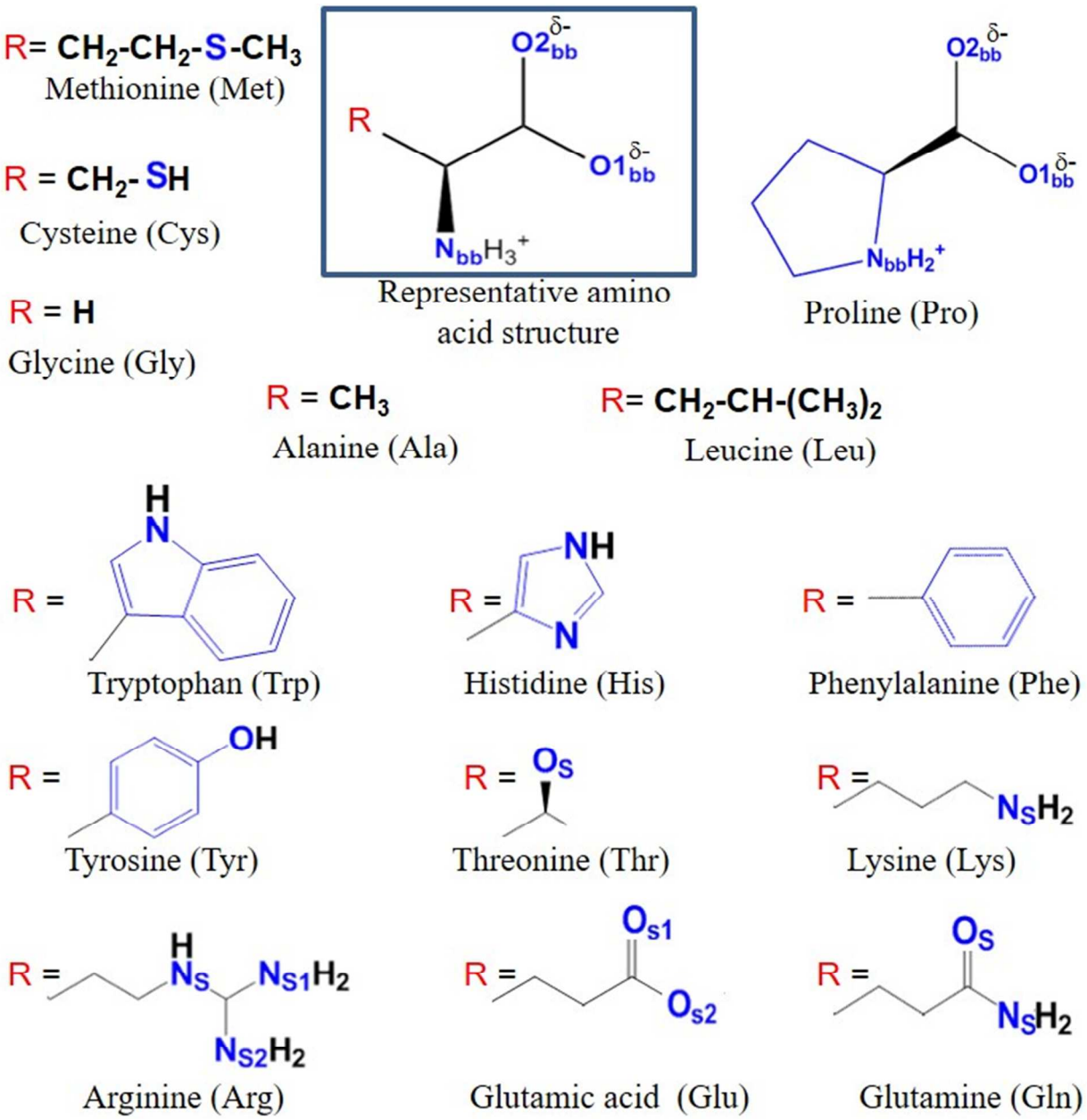

Figure 1: Potential interaction sites for respective amino acids. A representative structure for amino acids is shown with backbone atoms as interaction sites. The tagged sites in SMD simulations are shown in blue color for each amino acid.

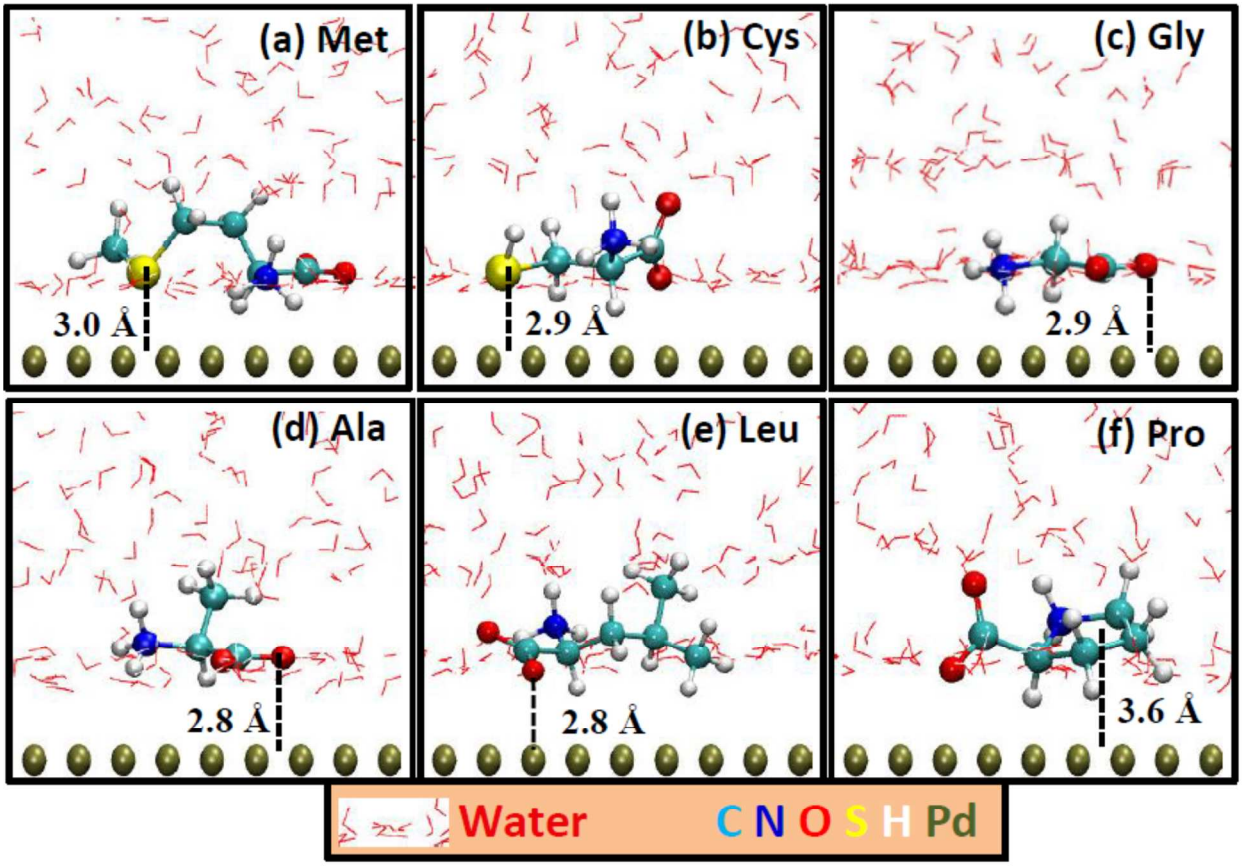

Figure 2: Orientations of S-containing amino acids; (a) Met, (b) Cys, and aliphatic amino acids (c) Gly, (d) Ala, (e) Leu, (f) Pro on the Pd (111) surface. The distances of preferred interaction site from the top of the metal surface are indicated in each case.

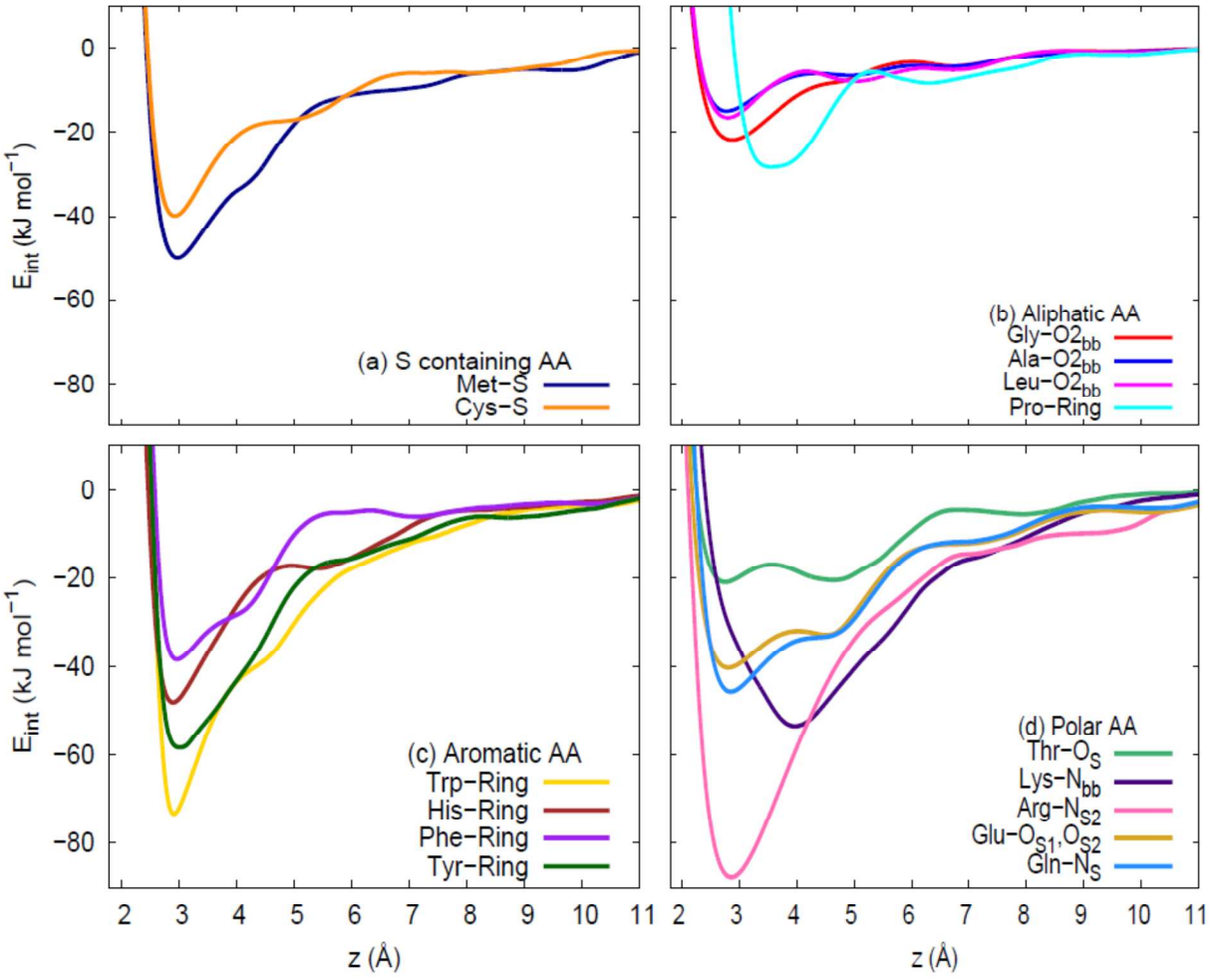

Figure 3: PMF profile as a function of the z coordinate for the interacting sites for the (a) aliphatic amino acids (Gly, Ala, Leu and Pro), (b) S-containing amino acids (Cys, Met), (c) aromatic amino acids (Trp, His, Phe and Tyr), and (d) polar amino acids (Thr, Lys, Arg, Glu and Gln) on the Pd (111) surface, as calculated from SMD simulations.

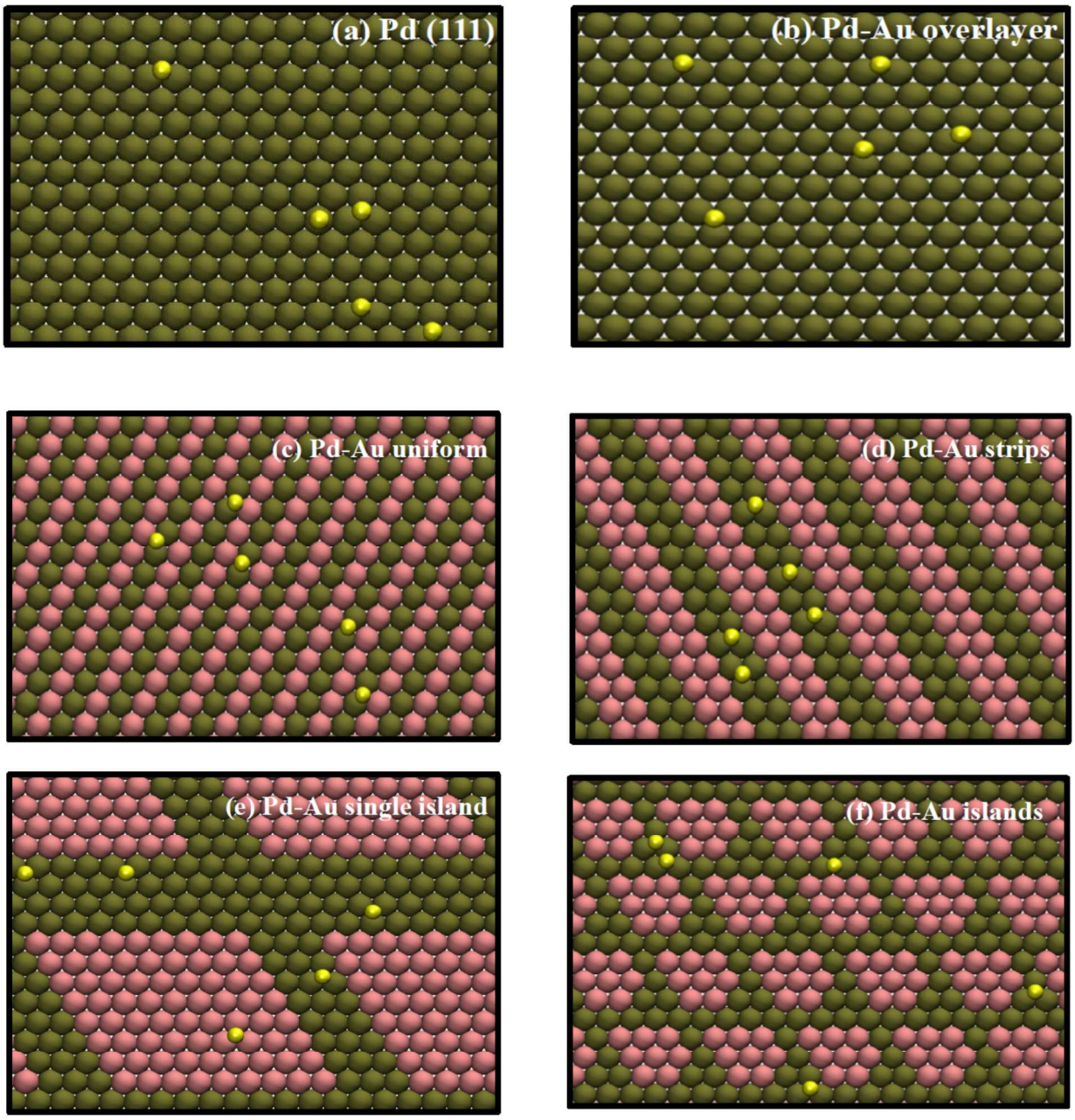

Figure 4: Positioning of S atom (yellow color) of Met as observed in five different simulations used for calculating the average E_{int} value on (a) Pd (111) surface, (b) Pd-Au overlayer, (c) Pd-Au uniform, (d) Pd-Au strips, (e) Pd-Au single island and (f) Pd-Au multiple islands. The tan and red colors indicate Pd and Au atoms, respectively.

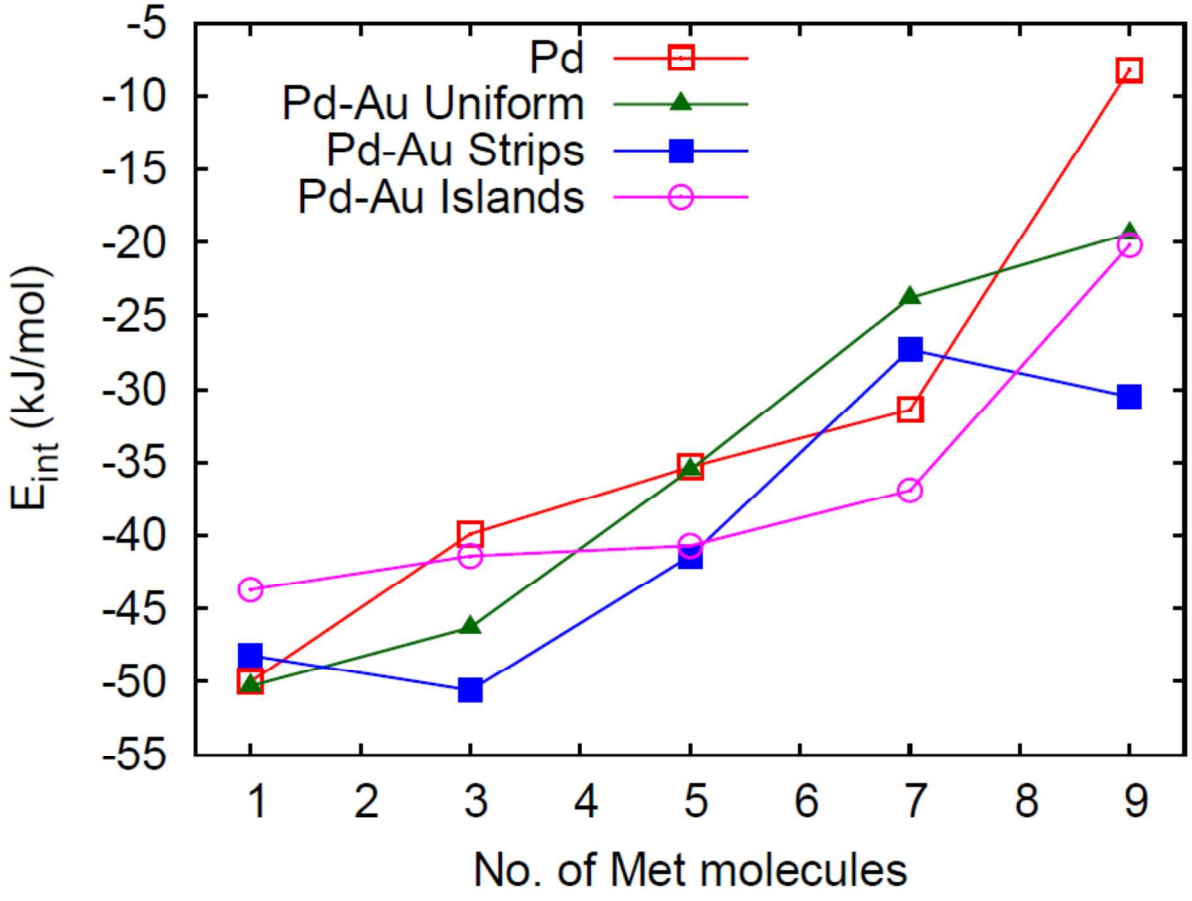

Figure 5: Variation of interaction energy, E_{int}, with the increase in coverage for Met interacting with the Pd (111) and different Pd-Au segregated surfaces.

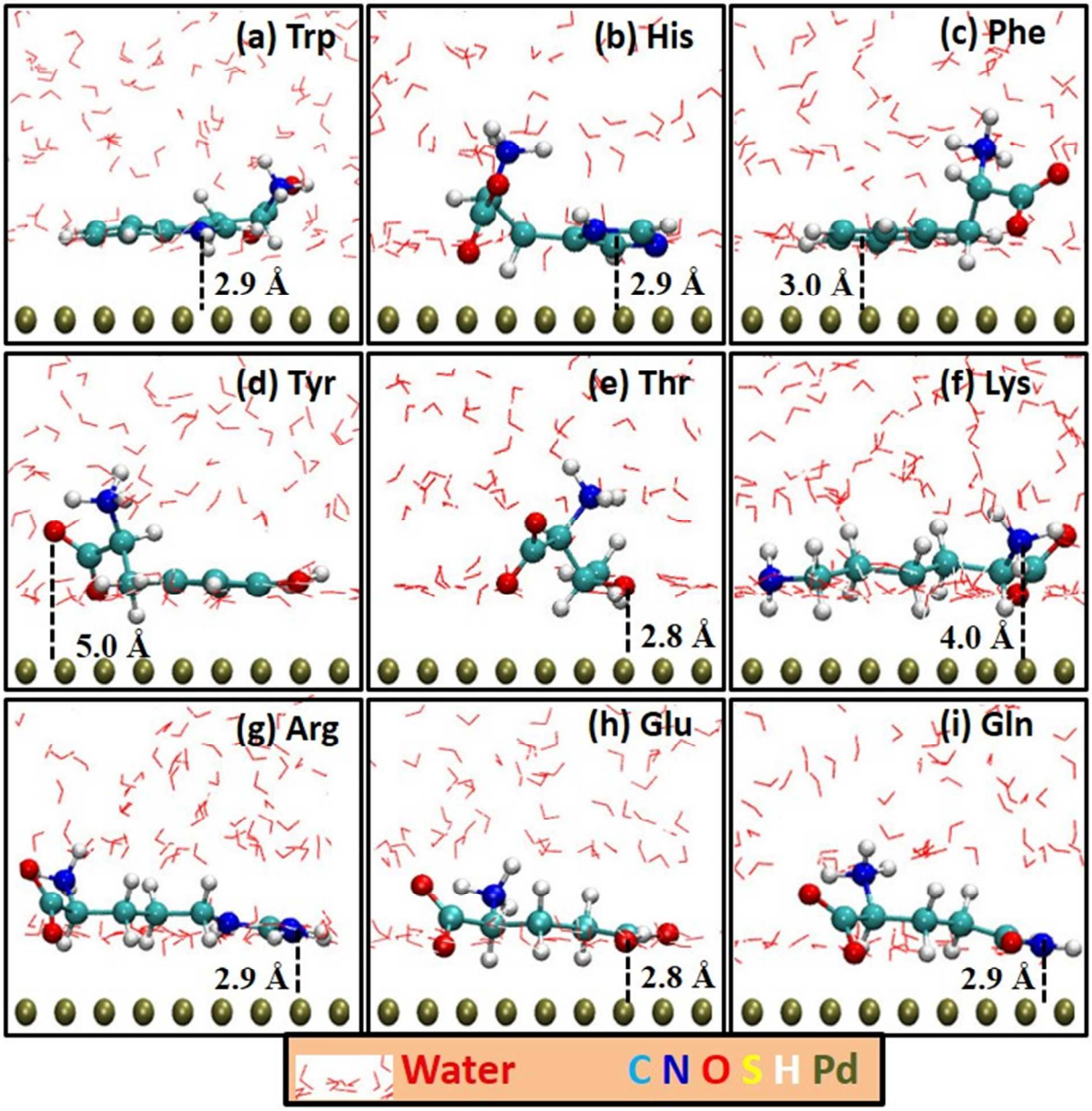

Figure 6: Orientations of aromatic amino acids; (a) Trp, (b) His, (c) Phe (d) Tyr and polar amino acids; (e) Thr, (f) Lys, (g) Arg, (h) Glu and (i) Gln on the Pd(111) surface. The distances of preferred interaction site from the top of the metal surface are indicated in each case.

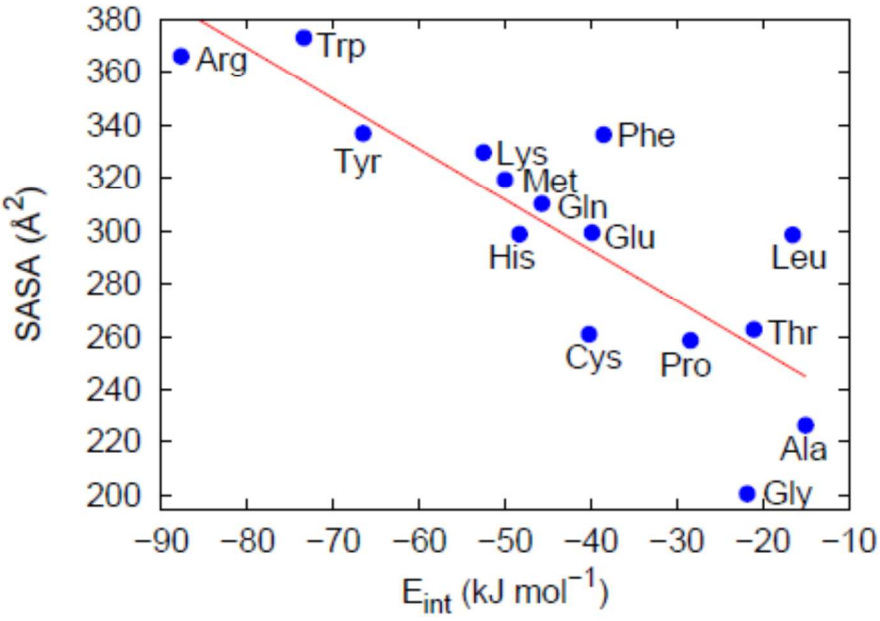

Figure 7: Solvent accessible surface area, SASA, as a function of E_{int}, via the preferred interaction site for each amino acid as obtained from MD simulations. The values were fitted to a straight line.

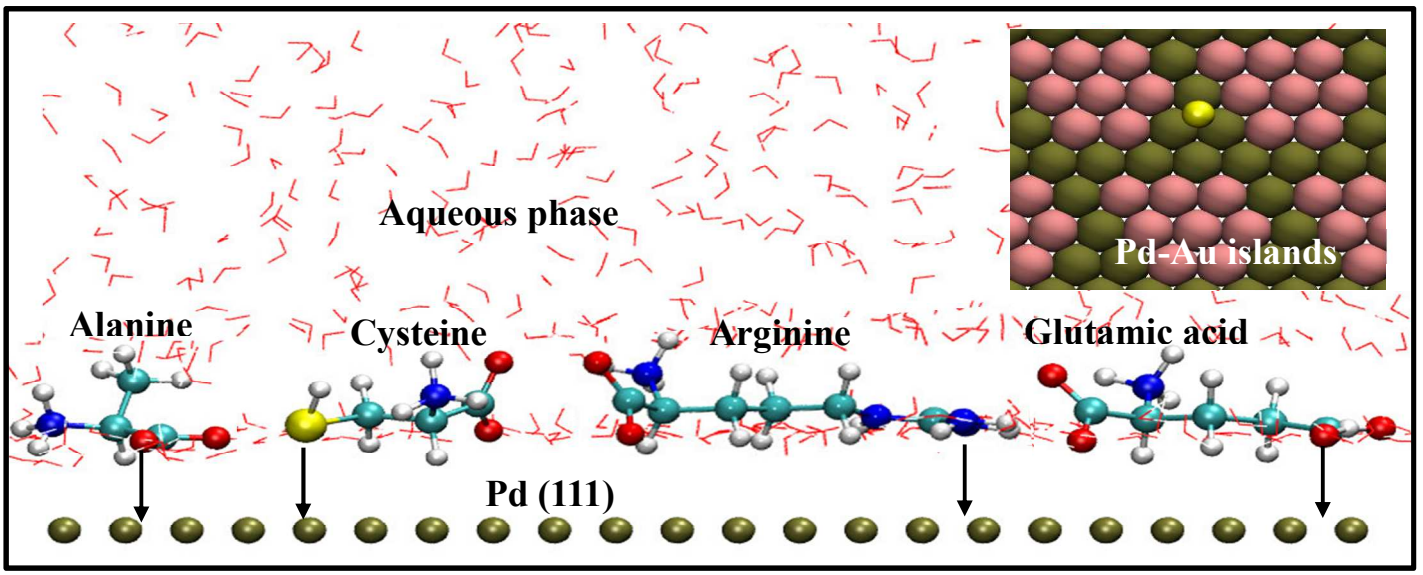

TOC Graphic: Interaction of different amino acids via the preferential interaction site with the metal surfaces.